Hollow core-shell structured mesoporous MWCNT/carbon nanofiber composites by electrospinning and silica template as counter electrodes for dye-sensitized solar cells

Seok-Hwan Park[a,b,c], Byung-Kwan Kim[a,b,c], Wan-Jin Lee[a,b,c*]

[a]School of Applied Chemical Engineering, Chonnam National University,
[b]Center for Functional Nano Fine Chemicals, Chonnam National University,
[c]Alan MacDiarmid Energy Research Institute, Chonnam National University,
Gwangju 500-757, Republic of Korea

ABSTRACT

The multi-walled carbon nanotube (CNT)-embedded carbon nanofibers (CNT/meso-HACNF) with hollow macroporous core/mesoporous shell structure are prepared by concentric electrospinning, and subsequent stabilization, carbonization, SiO_2 template etching, and activation. A sample without SiO2 template etching was defined as CNT/HACNF. Hollow core precursor was pyrolytic poly(methyl methacrylate) (PMMA), and carbon shell precursor was CNT/polyacrylonitrile (PAN) or fumed silica (SiO_2)/PAN or CNT/SiO_2/PAN. The CNT/meso-HACNF with hollow core/highly mesoporous shell structure represented large specific surface area and good electrical conductivity in employing as catalysts of counter electrodes (CE) for dye-sensitized solar cells (DSSCs) due to cocentric electrospinning, SiO_2 template etching, and proper thermal process. The CNT/meso-HACNF CE presents a high efficiency considering a Pt-free catalyst and and is comparable to Pt CE because of its hollow core/CNT-embeded highly mesoporous shell structure, which promote the electron and ion transfer and decrease the resistance of charge transfer owing to increasing the contact area between liquid electrolyte and CNT/meso-HACNF. Highly mesoporous CNT/meso-HACNF has a large surface area of 1033 m^2/g with a mesoporous surface area of 138 m^2/g. The efficiency of CNT/meso-HACNF increases to 6.73 %, but that of CNT/HACNF undeveloped with mesoporous structure to shell side shows 6.05 % due to without SiO_2 etching.

Keywords: Core-shell structure; mesopore; Carbon nanofibers; Electrospinning; Counter electrode; Dye-sensitized solar cell

1 INTRODUCTION

Dye-sensitized solar cells (DSSCs) have been fascinated in solving an energy problem due to their low production costs, and high energy conversion efficiency [1-3]. DSSCs consists of photoelectrode with tipycal TiO2 absorbed with the dye, the electrolyte, and the counter electrode (CE). Among them, the CE is an essential compoenent because it collects electrons arriving form the external circuit and catalyzing the reduction of triiodide ion (I_3^-). Platinum as the best performing material in the CE shows excellent electrocatalytic activity for the I_3^-/I^- redox couple, but is necessary to replace due to its expensiveness, and corrosive phenomena in the iodide electrolyte. To solve such a problem, various carbonaceous materials such as carbon nanotube, activated carbon, graphite, and carbon black have been used as an alternative CE due to their large surface area, high electronic conductivity, corrosion resistance towards iodine, high reactivity for triiodide reduction, and low cost [4-8]. However, the morphology of carbonaceous materials needs to be changed to maximize the photoelectrochemical performance by simultaneously possessing both excellent porous structure and 1-D conducting pathway with facile electron transfer. The concentric electrospinning is a unique method that can produce both CNT- and SiO_2- embedded nanofibers with hollow core/shell structure as a non-woven web. The performance of this method relies on how well PMMA of hollow core side sustains in the concentric fibers and both CNT and SiO2 distributes in shell side.A non-woven web obtained from concentric electrospinning can be prepared as CNT-embedded activated nanofibers web hollow coe/mesoporous shell structure with high electrical conductivity through stabilization, carbonization, SiO_2 template etching, and activation processes. The CNT/meso-HACNF used in this study has excellent characteristics for enhancing the photoelectrochemical performance due to the mesoporous structure, enhanced electrical conductivity, and formation of a good charge-transfer complex through concentric electrospinning, SiO_2 etching, and subsequent thermal process. The photoelectrochemical behavior was examined by comparing the CNT/HACNF, and Pt counter electrode.

2 EXPERIMENTAL

Polymethylmethacrylate (PMMA, Mw = 120,000, Aldrich Chem.), polyacrylonitrile (PAN, Mw = 150,000, Aldrich Chem.), and N,N-dimethylformamide (DMF, Aldrich Chem.) were used as a pyrolytic core precursor, a carbon shell precursor, and a solvent, respectively. The multi-walled carbon nanotubes (CNT, dia. 10-25 nm, length 10-50 nm, Iljin Nanotech Co., Korea) used as an electronic conductor, Hydrophilic fumed silica (SiO_2, 300 m^2/g, 15 nm, Konasil, K-300, DC Chemical Co., Korea) used as a template to improve mesoporous structure. The fabricating and I_3^- reduction process for CNT/meso-HACNF are shown in Figure 1. A dual concentric injection nozzle (inner nozzle: 22G, outer nozzle: 17G) was designed to prepare core (PMMA)/shell (CNT/PAN or CNT/SiO_2/PAN)

precursor nanofibers. For CNT/HACNF, and CNT/meso-HACNF, both core sides are consisted of the same amounts of 10 wt.% PMMA in DMF, and the composite solutions of shell sides are composed of 10 wt.% PAN/2 wt.% CNT, and 10 wt.% PAN/2 wt.% CNT/20 wt.% SiO_2 respectively in DMF. The condition of electrospinning is the same as the previous methods [9,10]. The flow rate of the inner (PMMA) and outer (PAN composite) spinning solutions in all samples preparation were 1 and 1.5 ml/h, respectively. All electrospun fibers were stabilized by keeping for 1 h after increasing to 280 ◦C at a rate of 1 ◦C/min in air, carbonized for 1 h at 800 ◦C in nitrogen. The silica etching for SiO_2 template embedded samples was repeated four times using a 2 M NaOH aqueous solution at room temperature. Afterwards, the activation was carried out by supplying 30 vol.% steam for 1 h at 800 ◦C in nitrogen.

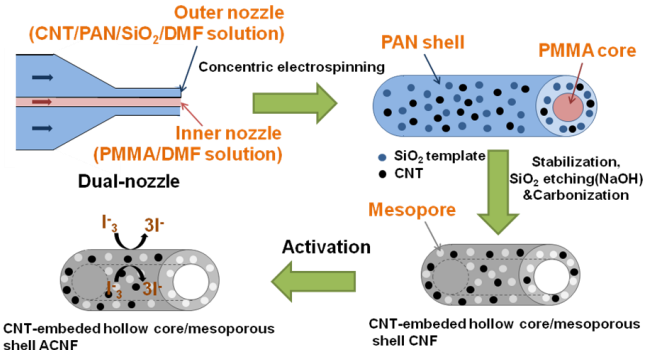

Figure 1: The simple preparing model and catalytic activity for CNT/meso-ACNF.

Before spray, all samples was grinded using a mortar for 30 min. After that, each 0.012 g grinded powder was added into 3 g isopropanol, and then the mixture was sonicated for 1 hr to make homogeneous slurry. After sonication, the mixture was directly sprayed onto the FTO substrate with a portable spray gun connected to the air compressor for 200 sec. The TiO_2 films on the FTO glass were prepared using the squeeze printing method with TiO_2 paste. The films were annealed at 500 ◦C for 30 min and then immersed in a 0.5 mM solution of N719 in ethanol for 24 h at room temperature. TiO_2 paste (Ti-nanoxide D, Solaronix, Switzerland) is used as a photoanode material. The layer thickness of TiO_2 was 8 μm. DSSCs were assembled by employing N719-sensitized nanoporous TiO_2 electrodes and various CEs. The liquid electrolyte comprising of 0.6 M DMPImI, 0.1 LiI, 0.05 M I_2, 0.5 M t-butylpyridine and acetonitrile solvent was dropped onto the nanoporous TiO_2 film, and then the TiO_2 eletrode was clipped firmly with the counter electrode. The active area of the DSSCs was 0.23 cm^2 The I-V curves of DSSCs were measured using the electrochemistry analyzer (Compactstat.e, Ivium Techn., Netherlands) under irradiation with simulated solar light from a 150W xenon arc lamp (PEC-L01, solar simulator, Peccell Tech., Japan). The incident light intensity was adjusted to 100 mW/cm (AM 1.5 G). The AC impedance spectra of the DSSCs were determined using the electrochemistry analyzer at the frequency range of 10 mHz ~ 100000 Hz with illumination. The magnitude of the alternative signal was 10 mV.

3 RESULTS AND DISCUSSION

The cross-sectional SEM and TEM images for CNT/HACNF, and CNT/Meso-HACNF are depicted in Figure 2. Both samples excellently sustain hollow core/shell structure, which is originated from immiscibility and thermal stability between PAN and PMMA during cocentric electrospinning and thermal process [11]. The CNT/HACNF possesses the smooth surfaces with hollow core and shell diameter of approximately 600 and 800 nm, but was not well developed in shell side. On the other hand, the CNT/Meso-HACNF with hollow core and shell diameter of approximately 500 and 900 nm has rough surface with a bent and wrinkled appearance. The CNTs are well distributed in shell and the mesoporous structure was well developed with a lot of tiny pit to both the rough surface and the inside due to SiO_2 template etching.

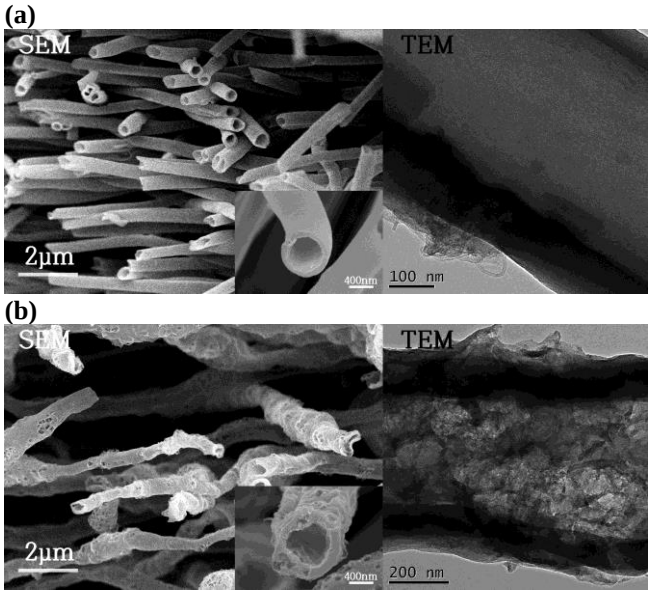

Figure 2: The cross-sectional SEM and TEM images for (a) CNT/HACNF, and (b) CNT/Meso-HACNF.

Raman spectra for CNT/HACNF, and CNT/Meso-HACNF are shown in Figure 3a. The D band at 1350 cm^{-1} originates from structural disorders and defects, the G band at 1580 cm^{-1} associates with the sp^2 vibration of a perfect graphite crystal [12,13]. The D/G intensity ratio of CNT/Meso-HACNF (ID/IG = 1.01) are smaller than that of CNT/HACNF (ID/IG = 1.12). The smaller D/G intensity ratio of CNT/Meso-HACNF is deeply related high specific surface area and mesoporous structure, facilitating the electron transfers at the counter electrode/electrolyte interface [8]. Figure 3b. shows nitrogen adsorption-desorption isotherms for CNT/HACNF, and CNT/Meso-HACNF. The CNT/HACNF shows a typical type I pattern with microporous structure. On the other hand, CNT/Meso-

HACNF represent a linear increase of the amount of adsorbed nitrogen at low pressure (P/P_0 = 0.3), and is classified as a typical IV isotherm with hysteresis confirming mesoporous evidence. In the inset image of Figure 2b, the BJH pore size distribution for CNT/Meso-HACNF shows a bimodal pore distribution with two distinctive peaks at ca. 70 and 120 nm due to the CNT and SiO_2 template etching [17]. The CNT/Meso-HACNF shows the excellent pore characteristics with mesopore average diameter of 18.6 nm and mesopore surface area of 138.2 m^2/g, whereas CNT/HACNF mesopore average diameter of 9.9 m^2/g and mesopore surface area of 69.2 m^2/g.

(a)

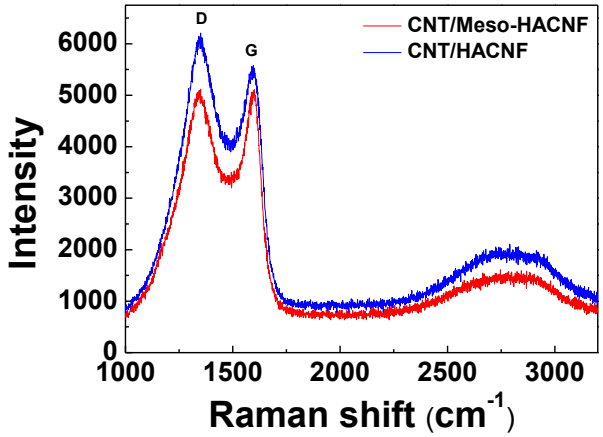

(b)

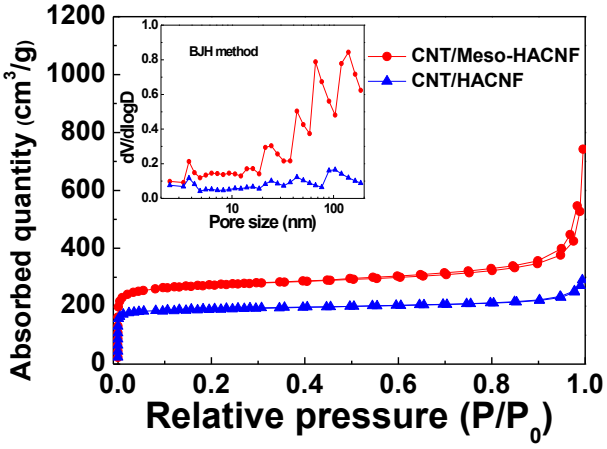

	Meso pore surface area. (m^2/g)	Total surface area (m^2/g)	Total pore volume (cm^3/g)	Meso pore avg. dia.[a] (nm)
CNT/HACNF	69.2	751.8	0.42	9.9
CNT/Meso-HACNF	138.2	1033.8	0.89	18.6

[a]Calculated with 4 V/A of BJH method.

Figure 3: (a) Raman spectra and (b) N_2 asorption isothermsand pore size distribution. The table offers extracted pore characteristics of CNT/HACNF, and CNT/Meso-HACNF.

The photocurrent-voltage curves of the cells with CNT/HACNF, CNT/Meso-HACNF, and Pt CEs are illustrated in Figure 4a. The J_{sc}, V_{oc}, fill factor (FF) and efficiency (η) of photovoltaic parameters derived from I-V curves are given in Table. The CNT/Meso-HACNF parameters are higher than that of CNT/HACNF, showing J_{sc} of 14.5 mA/cm^2, V_{oc} of 0.74 V, FF of 0.64, and η of 6.73 %, while CNT/HANF parameters depicts J_{sc} of 13.6 mA/cm^2, V_{oc} of 0.74 V, FF of 0.62, and η of 6.05 %, and Pt parameters represents J_{sc} of 15.6 mA/cm^2, V_{oc} of 0.74 V, FF of 0.62, and η of 7.12 %. The difference between CNT/Meso-HACNF and CNT/HACNF parameter is originated from the formation of mesoporous structure. By comparison, the values of J_{sc} for CNT/HACNF, and CNT/Meso-HACNF are lower than that of Pt CE. The low value of J_{sc} is ascribed to higher internal resistance due to both a large particle size and the opaque nature between CNF layers.

(a)

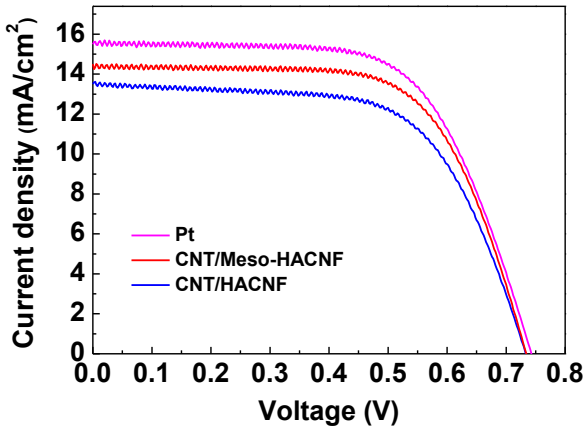

(b)

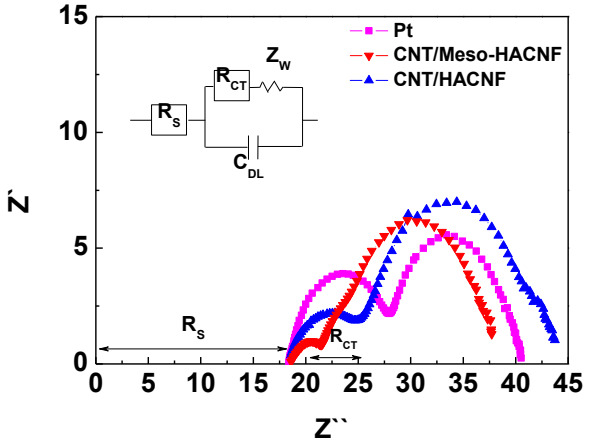

	J_{sc} (mA /cm^2)	V_{oc} (V)	FF	η (%)	R_S (Ω cm^2)	R_{CT} (Ω cm^2)
Pt	15.6	0.74	0.62	7.12	18.4	9.6
CNT/HACNF	13.6	0.74	0.62	6.05	18.6	6.2
CNT/Meso-HACNF	14.5	0.74	0.64	6.73	18.6	2.9

Figure 4: Electrochemical characterization of Pt, CNT/HACNF, and CNT/Meso-HACNF using (a) I-V curves and (b) EIS. The table offers extracted photovoltaic characteristics of the DSSCs.

The increased photoelectrochemical performance for CNT/Meso-HACNF CE maily originates from the following reasons. First, the hollow core/highly mesoporous shell structure prepared by cocentric electrospinnning leads to the facile charge transfer through promoting the I_3^-/I^- redox reaction rate by easily uptaking liquid electrolyte into numerous pores within the shell, hollow core, CNT, and macropores in CNF layers. Thus, the increase in contact area between CNT/Meso-HACNF and liquid electrolyte caused by the highly mesoporous structure promotes excellent I_3^-/I^- redox reaction [8,16]. Second, 1-D morphology of carbon nanofiebrs by electrospinning and high electrical conductivity of CNT facilitate charge transfer reaction by easy electron transfer [17]. EIS with their equivalent circuit for CNT/HACNF, CNT/Meso-HACNF, and Pt CEs are analyzed in Figure 4b. The R_{ct} for all samples are ranked as follows: CNT/Meso-HACNF (2.9 Ω cm^2) > CNT/HACNF (6.2 Ω cm^2) > Pt (9.6 Ω cm^2). The reason for this is that CNT/Meso-HACNF offers a higher catalytic performance initiated from higher surface area with hollow core/highly mesoporous shell structure, and 1-D morphology of carbon nanofibers. The internal serial resistance (R_s) is the onset point of the first semicircle for the high frequency region. The R_s represents mainly the sum of sheet resistance of the FTO glass substrate and the contact resistance of the counter electrode. Therefore, the R_s of Pt is lower than other samples due to high electrical conductivity.

4 CONCLUSIONS

The CNT/Meso-HACNF with hollow core/highly mesoporous shell structure were successfully prepared through concentric electrospinnning, and subsequent stabilization, carbonization, SiO_2 template etching, and activation. The hollow core structure of all samples perfectly sustained due to the effect of immiscibility and thermal stability. The CNT/Meso-HACNF with highly mesoporous structure represented total surface area of 1033.8 m^2/g with mesoporous surface area of 138.2 m^2/g, and total pore volume of 0.89 cm^3/g. The energy conversion efficiency (6.73 %) for CNT/Meso-HACNF CE is comparable to that of Pt CE (7.12 %). The R_{ct} of CNT/Meso-HACNF was the smallest with the value of 2.9 Ω cm^2 due to its higher catalytic performance, which originated from mesoporous structure and high electrical conductivity by CNT.

ACKNOWLEDGEMENT

This research was supported by International S&T Cooperation Program through the National Research Foundation of Korea (NRF) funded by the Ministry of Education, Science and Technology (MEST) (K2090300202412E010004010).

REFERENCES

[1] B. O'Regan, M. Grätzel, Nature, 353, 737, 1991.
[2] M.K. Nazeeruddin, A. Kay, I. Rodicio, R. Humphry-Baker, E. Mueller, P. Liska, N. Vlachopoulos, M. Grätzel, J. Am. Chem. Soc. 115, 6382, 1993.
[3] M. Grätzel, J. Photochem. Photobiol. A. 164, 3, 2004.
[4] K. Suzuki, M. Yamamoto, M. Kumagai, S. Yanagida, Chem. Lett. 32, 28, 2003.
[5] S.U. Lee, W.S. Choi, B.Y. Hong, Sol. Energ. Mater. Sol. Cells, 94, 680, 2010.
[6] K. Imoto, K. Takatashi, T. Yamaguchi, T. Komura, J. Nakamura, K. Murata, Sol. Energ. Mater. Sol. Cells, 79, 2003, 459.
[7] T.N. Murakami, S. Ito, Q. Wang, M.K. Nazeeruddin, T. Bessho, I. Cesar, P. Liska, R. Humphry-Baker, P. Comte, M. Grätzel, J. Electrochem. Soc. 153, A2255, 2006.
[8] G. Wang, C. Huang, W. Xing, S. Zhuo, Electrochim. Acta, 56, 5459, 2011.
[9] Y.W. Ju, G.R. Choi, H.R. Jung, C. Kim, K.S. Yang, W.J. Lee, J. Electrochem. Soc. 154, A192, 2007.
[10] Y.W. Ju, J.H. Park, H.R. Jung, W.J. Lee, Electrochim. Acta, 52, 4841, 2007.
[11] C. Kim, Y.I. Jeong, B.T.N. Ngoc, K.S. Yang, M. Kojima, Y.A. Kim, M. Endo, J.W. Lee, Small, 3, 91, 2007.
[12] H. Pan, C.K. Poh, Y.P. Feng, J. Lin, Chem. Mater. 19, 6120, 2007.
[13] P. Lian, X. Zhu, S. Liang, Z. Li, W. Yang, H. Wang, Electrochim. Acta, 55, 3909, 2010.
[14] G. Veerappan, K. Bojan, S.W. Rhee , ACS Appl. Mater. Interfaces, 3, 857, 2011.
[15] G. Veerappan, W. Kwon, S.W. Rhee, J. Power Sources, 196, 10798, 2011.
[16] G. Wang, W. Xing, S. Zhuo, J. Power Sources, 194 , 568, 2009.
[17] S.H. Park, H.R. Jung, B.K. Kim, W.J. Lee, J. Photochem. Photobiol. A. 246, 45, 2012.1

CORRESPONDING AUTHOR FOOTNOTE:
*Prof. Wan-Jin Lee, E-mail: wjlee@jnu.ac.kr,
Telephone +82-62-530-1895, Fax +82-62-530-1889